ACS OMEGA

http://pubs.acs.org/journal/acsodf

Article

Construction of Macromolecules of Depolymerized Lignite

Muxin Liu, Zhiping Lei, Xianzhong Cao, Jingchong Yan,* Hengfu Shui,* Zhicai Wang, Jiabao Hu, and Mengqi Hong

Cite This: *ACS Omega* 2023, 8, 22820−22826

Read Online

ACCESS | Metrics & More | Article Recommendations

ABSTRACT: Preparing ash-less coal and further converting it into chemicals is an efficient and promising means for lignite utilization. This work performed depolymerization of lignite to prepare ash-less coal (SDP) and separated it into the hexane-soluble fraction (HS), toluene-soluble fraction (TS), and tetrahydrofuran-soluble fraction (THFS). The structure of SDP and those of subfractions were characterized by elemental analysis, gel permeation chromatography, Fourier transform infrared spectroscopy, and synchronous fluorescence spectroscopy. The results show that SDP is a mixture of aromatic derivatives containing alkyl substituents and oxygen-containing functional groups. The number of condensed aromatic rings, the amount of oxygen-containing functional groups, and the molecular weight gradually increase as HS < TS < THFS. SDP was further analyzed by ^{1}H-NMR and ^{13}C-NMR to calculate its structural parameters. The macromolecule of THFS contains 15.8 total ring systems with 9.2 aromatic rings and 6.6 naphthenic rings. On average, each THFS molecule contains 6.1 alcohol hydroxyl groups, 3.9 phenol hydroxyl groups, 1.4 carboxyl groups, and 1.0 inactive oxygen-containing functional groups. The dominant reactions occurred during depolymerization are the breakage of ether linkages. The average THFS molecule consists of 3.3 structural units with aromatic nuclei (2.8 rings on average) linked with methylene, naphthene, and so forth.

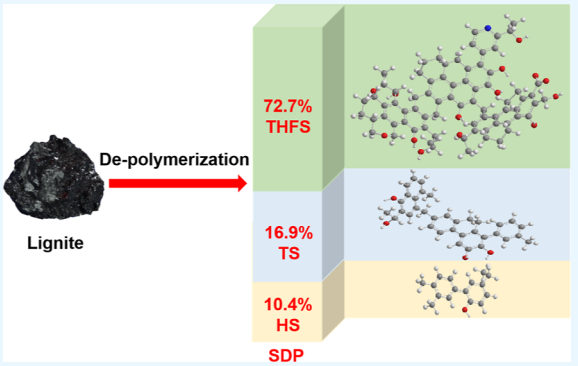

1. INTRODUCTION

Lignite is an important energy resource due to its enormous reserves, which exceeds 130 billion tons for China. Therefore, it is necessary and significant to realize clean and value-added utilization of lignite. However, lignite is inferior fuel for boilers to produce electricity because of its high moisture (18−24%) and ash (16−26%) content, as well as its relatively low net calorific value (3281−3854 kcal·kg^{-1}).[1] On the other hand, lignite is promising for preparing ash-less coal (also known as HyperCoal in the literature) due to its high activity and low cost. HyperCoal is a coal derivative with very low mineral content obtained from coal after solvent extraction or deashing.[2−4] Compared with coal, HyperCoal shows many advantages in the process of transformation and utilization. For example, HyperCoal can be liquefied without coke formation and give much higher conversions and oil yields, and the catalyst is not deactivated and recyclable.[3,5,6] The catalytic gasification of HyperCoal demonstrated a much higher gasification rate than that of raw coals at lower temperatures, and the catalyst is not deactivated.[7] In addition, HyperCoal can be directly injected into gas turbines to generate power,[8] used for coal blending coking to improve the coke strength,[9,10] or used to prepare activated carbon for electric double-layer capacitors.[11]

The most common technology to produce HyperCoal is to separate organic matter and minerals in coal by solvent extraction, but the extraction yield of lignite is low because of the rich hydrogen bonds in lignite.[6,12] It has been reported that coal can be effectively depolymerized by reacting with sodium hydroxide and alcohol to obtain the decomposition product (SDP), which is similar to HyperCoal. Due to the depolymerization effect of NaOH on the structure of coal, the yield of SDP is higher than that of HyperCoal prepared by extraction. Ouchi et al.[12] studied the depolymerization of coal with NaOH in 10 kinds of alcohols and found that the yield of soluble pyridine is higher than 80%. Makabe et al.[13] studied the reaction of coal with NaOH in ethanol and found that the yield of soluble pyridine varied at 80−98% and increased with temperature and NaOH concentration. Bimer et al.[14] found that the yield of the soluble product from Janina coal was 85.5% due to the NaOH−methanol treatment at 350 °C. Our

Received: March 16, 2023
Accepted: May 30, 2023
Published: June 9, 2023

Table 1. Ultimate and Proximate Analyses of SL Lignite and SDP[a]

	proximate analysis (wt %)			ultimate analysis (wt %, daf)				
	M_{ad}	Ash_d	VM_{daf}	C	H	O[b]	N	S
SL lignite	15.0	18.3	49.5	67.95	4.50	24.78	0.98	1.29
SDP	4.6	0.0	68.6	75.44	6.87	15.57	0.98	1.14

[a]M: moisture; VM: volatile matter; ad: air-dried; d: dry; daf: dry-ash-free. [b]By difference.

previous work showed that Shengli (SL) lignite can be efficiently converted into SDP with a yield exceeding 99%.[1]

Because SDP reserves aromatic structures of coal, it can be a potential material for production of aromatics and aromatic derivatives. To realize this purpose, a detailed understanding of the structure of SDP is required to select a reasonable SDP processing means and accurately control the conversion process. However, up to now, little information is available on SDP structural features, leading to limited and less-efficient use of SDP. Besides, the studies about the structural characterization of SDP can contribute to the understanding of the coal structure due to the information on the coal structure retained by SDP.

Similar to heavy products such as heavy oil, asphaltene, and preasphaltene, SDP is a complex macromolecular mixture. The commonly used structural characterization methods for these heavy products, such as elemental analysis, FTIR spectroscopy, GPC analysis, synchronous fluorescence spectra, and nuclear magnetic resonance, often obtain one-sided information.[3,6,15,16] The integration of this information is the key to constructing the macromolecules of SDP. The calculation of structural parameters with the Brown−Ladner method can integrate the information obtained by these analysis methods to construct the macromolecules of heavy products.[17,18] For instance, Zhang et al.[19] calculated the average structural parameters by the modified Brown−Ladner method to understand the millisecond pyrolysis behavior of heavy oil over the solid base catalyst from the near-molecular level and the relationship between the structural composition and the solid base catalytic cracking behavior of heavy oil. Shao et al.[20] studied the structural characterization of asphaltene from the hydrotreatment of low-temperature coal tar under various pressures by the Brown−Ladner method and found that the naphthenic ring number remains almost unchanged, while the aromatic ring number reduced with pressure, demonstrating that the ring-opening rate of the naphthenic ring is slightly larger than the hydrogenating rate of the aromatic ring. Guo et al.[21] correlated the peak temperatures of the DTA curves during combustion with the number of aromatic rings per unit structure of coal and char obtained by the Brown−Ladner method and found that the peripheral parts of aromatic clusters are the active sites. Therefore, the Brown−Ladner method can be used for the structural characterization of SDP. It is important to note that, as a derivative of lignite, SDP probably contains more oxygen-containing functional groups. However, the Brown−Ladner method does not involve quantitative analysis of oxygen-containing functional groups, and how to quantitatively analyze these oxygen-containing functional groups is also an important problem to be solved.

To realize clean and value-added utilization of lignite, SDP was prepared by depolymerization of SL lignite and was subsequently separated into three subfractions by solvent extraction in this work. To understand the detailed structural characterization of SDP, the structure of subfractions was characterized by elemental analysis, FTIR spectroscopy, GPC, and synchronous fluorescence spectroscopy. The dominant fraction (THFS) of SDP was further characterized by ^{1}H-NMR and ^{13}C-NMR, and its structural parameters were calculated by the modified Brown−Ladner method. This study not only can facilitate the development of efficient lignite utilization but also deepens the understanding of the lignite structure and the depolymerization mechanism of lignite.

2. EXPERIMENTAL SECTION

2.1. Materials. A Chinese SL lignite was used in this work. The coal sample was ground to less than 74 μm and dried in vacuum at 110 °C for 24 h. Its ultimate and proximate analyses are listed in Table 1.

2.2. Preparation Procedures of SDP. Depolymerization of SL lignite was carried out in a 50 mL autoclave. 5.0 g of the dried coal loaded with 5.0 g of NaOH was charged into the reactor together with 15 mL of methanol. Before the test, the autoclave was sealed and flushed three times with N_2 followed by tuning the system to the desired initial pressure of 0.1 MPa. The autoclave was heated from room temperature to 300 °C for 10 min with stirring and then maintained at 300 °C for 60 min. Afterward, the autoclave was cooled rapidly to room temperature by pumping the water into the jacket of the autoclave. Although a small amount of gas products is generated with a yield of about 10 wt %, the focus of this article is on solid products. The reaction mixture was removed by washing it with methanol. The solid products were obtained by removing methanol through rotary evaporation. Then, the reaction products were acidified with a HCl solution (1 mol L^{-1}), followed by filtration. The solid product was extracted by tetrahydrofuran (THF) in the Soxhlet apparatus. Then, SDP was obtained by removing THF through rotary evaporation followed by drying under vacuum at 80 °C for 12 h. SDP was extracted with *n*-hexane and toluene sequentially in the Soxhlet apparatus. The *n*-hexane-soluble, *n*-hexane insoluble/toluene-soluble, and toluene-insoluble/THF-soluble fractions obtained are defined as HS, TS, and THFS, respectively. After drying, the subfractions were quantified and their yield was 10.4, 16.9, and 72.7%, respectively. The ultimate and proximate analyses of SDP are listed in Table 1.

2.3. Characterizations of SDP. The elemental analysis was performed at the mode of CHNS using a Vario EL III elementary analyzer. The SL lignite and SDP subfractions were characterized by FTIR spectroscopy using a PE-Spectrum One IR spectrometer at ambient temperature. In the FTIR measurements, the sample was mixed with KBr at a mass ratio of 1:100 and the mixture was pressed into a pellet. GPC analysis was carried out on Shimadzu LC-20AT high-performance liquid chromatography (HPLC) with a Shimpack GPC-8025 (300 mm length, 0.8 cm i.d.) separation column isothermally at 25 °C. THF was used as the mobile phase with a flow rate of 1.2 mL·min^{-1}. Synchronous fluorescence spectra were recorded on a Hitachi F-4600 spectrophotometer with a 150 W xenon lamp as the excitation source. The difference

https://doi.org/10.1021/acsomega.3c01768
ACS Omega 2023, 8, 22820−22826

between excitation and emission wavelength was 14 nm. The spectral measurement at room temperature was made with the use of a quartz cell of a 1 cm path length. The samples were dissolved in THF, and the concentration was 5 $\mu g \cdot mL^{-1}$. A 10 mg solid sample (THFS) was dissolved in 0.6 mL of DMSO-d_6 and added with a few drops of TMS as an internal reference. The solution was then subjected to ^{1}H-NMR and ^{13}C-NMR analysis, which were recorded on a Bruker AV 400 MHz spectrometer at 25 °C.

3. RESULTS AND DISCUSSION

3.1. Elemental Analysis. The elemental analysis of the SDP subfractions is shown in Table 2. Compared to SL lignite, the SDP subfractions have higher H content and lower O content, which is caused by the destruction of oxygen-containing functional groups during depolymerization. Besides, THFS has the highest O content (16.43%), while HS has the lowest O content (9.43%) and the highest C content (81.69%), indicating the abundant oxygen-containing functional groups in THFS but rich hydrocarbon structures of HS. TS exhibits a similar C and O content to that of THFS, but its H content approximates that of HS.

Table 2. Elemental Composition (wt %) of SDP Subfractions

subfraction	C	H	O[a]	N	S
HS	81.69	7.95	9.43	0.68	0.25
TS	75.81	7.84	14.31	1.07	0.79
THFS	74.33	6.52	16.43	1.54	1.18

[a]By difference.

3.2. GPC Analysis. The number-average molecular weight (M_n) of the SDP subfractions is obtained from the GPC analysis as shown in Figure 1. The M_n of HS, TS, and THFS are 228, 537, and 1267, respectively, which are similar to those of oil, asphaltene, and preasphaltene from direct coal liquefaction. The molecular weight distribution range of HS is small, indicating its relatively simple compositions. However, the molecular weight distribution range of THFS is wide and its average molecular weight is large, indicating that THFS consists of complex macromolecules inheriting structural features of lignite. As THFS is the dominant subfraction of SDP, the structural features of SDP and SL lignite can be revealed by detailed analysis of the THFS fraction.

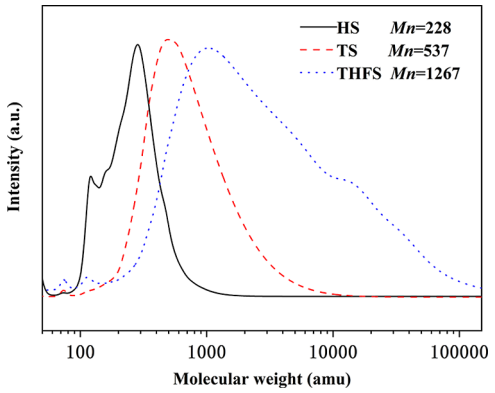

Figure 1. GPC curves of SDP subfractions.

3.3. FTIR Analysis. Figure 2 shows the FTIR spectra of SL lignite and SDP subfractions. It can be seen that SL lignite and the SDP subfraction all have clear O−H stretching signals at 3400 cm^{-1}. The peak strength of THFS and TS is strong while that of HS is weak, indicating that THFS and TS contain more hydroxyl groups, which is consistent with the oxygen O content in Table 2. The bands at 3000−2800 cm^{-1} are assigned to aliphatic C−H stretching vibrations and can be used to determine the aliphatic hydrogen content.[22,23] The corresponding peaks for HS and TS are strong while that for THFS is weak, indicating that HS and TS contain more alkane structures. This is consistent with their higher C and H content in Table 2. All the SDP subfractions show the obvious carbonyl vibration peaks at 1710 cm^{-1}.[24,25] The peaks near 1610, 1500, and 1450 cm^{-1} are assigned to aromatic ring stretching vibrations.[16,25] The peaks of THFS and TS at these positions are strong while that of HS is weak, indicating abundant aromatic structures in THFS and TS. The bands at 1300−1000 cm^{-1} are assigned to C−O (alcohol), C−O (phenol), and C−O−C structures,[25] and their presence suggests the rich alcohol, phenol, and/or ether group in SDP subfractions. Comparatively, more oxygen-containing functional groups in their molecules are observed in THFS and TS, which are in accordance with the results of Table 2. Moreover, the reduced peak at 1030 cm^{-1} for the SDP subfractions compared to SL lignite indicates the destruction of ether linkage during the depolymerization process.[1,26]

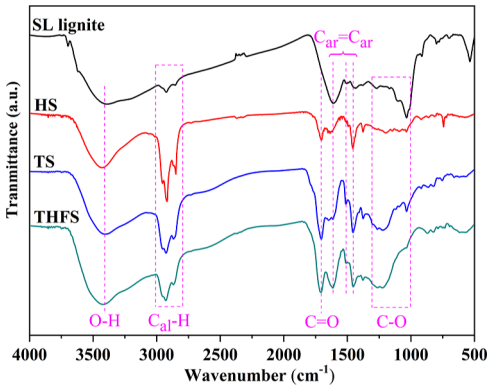

Figure 2. FTIR spectra of SL lignite and SDP subfractions.

3.4. Synchronous Fluorescence Spectroscopy Analysis. Synchronous fluorescence spectroscopy has been successfully applied to investigate the aromatic ring distribution of aromatic hydrocarbons such as heavy oil, extract products of coal, and coal-derived liquids. Assignment of the different bands was determined as shown in Figure 3 based on the work of Zou, Wang, and Katoh et al.[6,27,28] Clearly, HS primarily consists of a 1-ring aromatic nucleus and a small number of 2- and 3-ring condensed aromatic nuclei. The molecular weights of benzene, naphthalene, and anthracene are 78, 128, and 178, respectively, which are lower than the M_n of HS, indicating that the HS molecule has more substituents or contains multiple aromatic rings connected by linkages. TS is mainly composed of a 1-ring and 2-ring aromatic nucleus, followed by the 3-ring aromatic nucleus, and a small amount of the four-ring aromatic nucleus. THFS mainly has a 1−3 ring aromatic nucleus, followed by a 4-ring nucleus and above the aromatic nucleus. The overlapped spectra and numerous combinations of different structures indicate that THFS is a

https://doi.org/10.1021/acsomega.3c01768
ACS Omega 2023, 8, 22820−22826

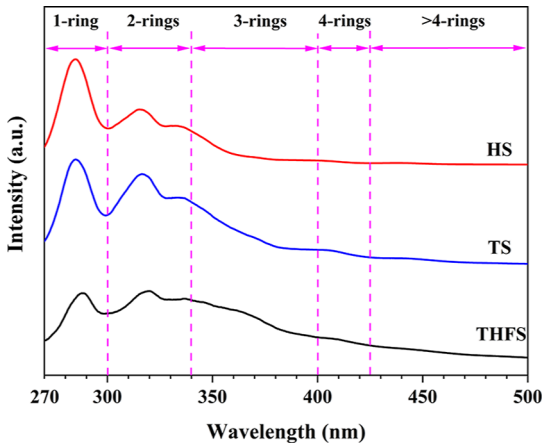

Figure 3. Synchronous fluorescence spectra of SDP subfractions.

complex mixture of various macromolecules. The above analyses indicate the condensed aromatic structures, large molecular weight, and abundant oxygen-containing groups of the SDP fraction and also imply its analogous structures with SL lignite.

3.5. Analysis of ^{1}H-NMR Spectroscopy. Figure 4a shows the ^{1}H-NMR spectra of the THFS fraction of SDP. Elemental

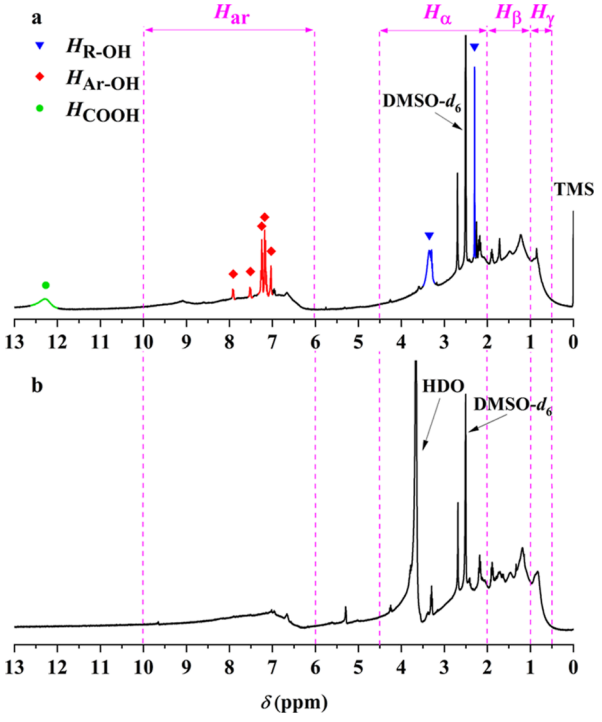

Figure 4. ^{1}H-NMR spectra of THFS: (a) THFS; (b) THFS after D_2O exchange.

analysis and FTIR spectroscopy show that THFS contains higher O contents and abundant oxygen-containing groups. The oxygen-containing functional groups containing active hydrogen, such as alcohol hydroxyl, phenol hydroxyl, and carboxyl, can be identified and quantified by the ^{1}H-NMR spectra before and after adding D_2O. Figure 4b shows the ^{1}H-NMR spectrum of the THFS fraction after a D_2O exchange experiment. The peaks of active hydrogen in the hydroxyl and carboxyl groups disappear; thus, the signals at 12.1, 7.3–7.0, 3.6, and 2.3 ppm in Figure 4a are assigned to carboxyl groups (COOH), phenolic hydroxyl groups (Ar–OH), and alcoholic hydroxyl groups (R–OH), respectively.

Figure 4b shows that THFS after D_2O exchange exhibits strong aliphatic hydrogen (0.5–4.5 ppm) but weak aromatic hydrogen (6.0–10.0 ppm). Aliphatic hydrogen can be further divided into α hydrogen (2–4.5 ppm), β hydrogen (1–2 ppm), and γ hydrogen (0.5–1 ppm). Similar assignments were widely used by researchers to study the ^{1}H-NMR spectra of coal-derived materials and heavy fractions of petroleum.[17,29] Through detailed analysis, the signals at 4.25 and 3.3 ppm are assigned to bridge protons at the α position to the aromatic ring. Peaks at 2.7 and 2.2 ppm indicate the presence of methyl groups attached to the aromatic ring in THFS with different chemical environments. The signals at 1.0 and 2.0 ppm are assigned to β-CH_3, β-CH_2, and β-CH to the aromatic ring, β-CH_2 and β-CH in the hydroaromatic structures, straight-chain alkane methylene protons, protons in the CH_2 groups of cycloparaffins, as well as protons in the CH groups of saturated hydrocarbons. The γ hydrogen region (0.85 ppm) corresponds to γ-CH_3 on the aromatic ring and straight-chain or alkane branch methyl protons.[18,29]

The average molecular formulae of THFS can be determined as $C_{78.5}H_{82.6}O_{13}N_{1.4}S_{0.50}$ based on the elemental composition of THFS in Table 2 and its M_n. Thus, the number of H atoms per THFS molecule (H_t) is 82.6. Thus, the number of various kinds of H can be determined from ^{1}H-NMR (Figure 4) and H_t. The percentage and number of each kind of hydrogen of THFS are shown in Table 3. Clearly, THFS

Table 3. Percentage and Number of Each Kind of Hydrogen of THFS

categories	definition	range in the ^{1}H-NMR spectrum (ppm)	proportion in total hydrogens (%)	number of each kind of hydrogen
H_{ar}	total number of aromatic hydrogen atoms per molecule	6–10	17.4	14.4
H_{al}	total number of aliphatic hydrogens per molecule	0.5–5	68.8	56.9
H_α	number of α hydrogens	2–4.5	25.0	20.7
H_β	number of β hydrogens	1–2	33.8	27.9
H_γ	number of γ hydrogens	0.5–1	10.0	8.3
H_{Ar-OH}	number of hydrogens in phenolic hydroxyl groups	7.0–7.3	4.7	3.9
H_{R-OH}	number of hydrogens in alcoholic hydroxyl groups	2.3, 3.6	7.4	6.1
H_{COOH}	number of hydrogens in carboxyl groups	12.1	1.7	1.4

contains plentiful aliphatic rings and alkyl side chains, and the substitution degree of aromatic rings is high. The aliphatic hydrogen mainly includes β and α hydrogen, accounting for 25.0 and 33.8% of the H_t, respectively. The major oxygen-containing functional groups are the phenolic and aliphatic hydroxyl groups.

The quantity of R–OH, Ar–OH, and COOH in THFS can be calculated with the number of corresponding active hydrogens, and then the amount of oxygen in phenolic and

https://doi.org/10.1021/acsomega.3c01768
ACS Omega 2023, 8, 22820–22826

alcoholic hydroxyl groups as well as carboxyl groups can be obtained. The total number of oxygen atoms (O_t) in the average THFS molecule is 13. After deducting the oxygen in the carboxyl group and hydroxyl group, the remaining oxygen can be ascribed to the inactive oxygen-containing functional group (e.g., ether bond). The number of various oxygen-containing functional groups and the distribution of oxygen in the THFS average molecule are shown in Table 4. Obviously,

Table 4. Number of Oxygen-Containing Functional Groups and Oxygen Distribution of THFS

categories	definition	proportion in total oxygens (%)	number of oxygen-containing function groups
N_{ar-OH}	number of phenolic hydroxyl groups		3.9
N_{R-OH}	number of alcoholic hydroxyl groups		6.1
N_{COOH}	number of carboxyl groups		1.4
$N_{O,in}$	number of inert oxygen functional groups		1.0
O_{Ar-OH}	number of oxygens in phenolic hydroxyl groups	28.3	3.9
O_{R-OH}	number of oxygens in alcoholic hydroxyl groups	44.2	6.1
O_{COOH}	number of oxygens in carboxyl groups	20.3	2.8
O_{in}	number of inert oxygens	7.2	1.0 (calculated as ether bonds)

the oxygen in a THFS average molecule is mainly distributed in the alcohol and phenol hydroxyl group, which is consistent with the strong peak at 3400 cm^{-1} in Figure 2. The inactive oxygen-containing functional groups in coal and its derivatives are mainly ether bonds. However, the number of inactive oxygen in THFS is very small, and only one inactive oxygen atom in the THFS molecule is observed. This result implies the cleavage of the ether bond during depolymerization, which is also verified by the reduced peak strength at 1030 cm^{-1} in Figure 2 (SL lignite and THFS).

3.6. Analysis of ^{13}C-NMR Spectroscopy. Figure 5 shows the corresponding ^{13}C-NMR for THFS. Evidently, some major resonance bands centered at 17.7, 21.5, 23, 29−29.5, 31, and 49 ppm are observed at the aliphatic region (15−70 ppm); besides, some primary resonances at 125−129 and 137 ppm appear in the aromatic regions (70−170 ppm).[30−33] The peak

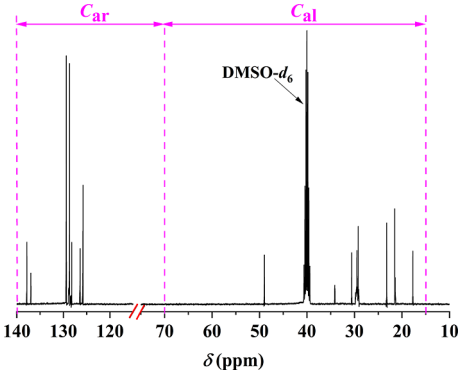

Figure 5. ^{13}C-NMR spectra of THFS.

at 17.7 ppm is assigned to methyl carbons of aliphatic structures. The signals at 22 and 23 ppm indicate the presence of methyl groups attached to aromatic rings.[30] The ones at 29−29.5 ppm are ascribed to methylene carbon of the naphthenic structure. The strong resonance peaks at 126−128.5 ppm indicate the preponderance of phenanthrene, its methyl-substituted molecule, and anthracene. The peaks at 137−139 ppm are attributed to polycyclic species and their substituted aromatics.[24,34] The total number of carbons (C_t) in THFS is 78.5; therefore, the number of each type of carbon of THFS can be calculated from the ^{13}C-NMR spectra, and the results are listed in Table 5. The number of carbons in the

Table 5. Percentage and Number of Each Kind of Carbon of THFS

categories	definition	range in the ^{1}C-NMR spectrum (ppm)	proportion in total carbons (%)	number of each kind of carbon
C_{ar}	total number of aromatic carbons atoms per molecule	70−170	57.0	44.7
C_{al}	total number of aliphatic carbons per molecule	13−70	41.2	32.3
C_{COOH}	number of carbons in carboxyl groups		1.8	1.4

carboxyl group of an average molecule of THFS is 1.4 (Table 4). Since the carboxyl carbon appears at 70−170 ppm, the integrated area of the carboxyl carbon should be deducted from aromatic carbon. It indicates that approximately 57.0% of total carbons presented in THFS exist in the form of aromatic species, and the aromatic hydrogen content is only 17.4%. In other words, the THFS mainly consists of condensed aromatic structures or aromatic structures with more substituents.

3.7. Construction of Molecular Models of THFS. The average structures of THFS can be obtained using the modified Brown−Ladner methods.[17,18] The major structural parameters are given in Table 6. Notably, the total number of N and S atoms (expressed in N_t and S_t) in the THFS molecule is 0.4 and 0.5, respectively. Since THFS is obtained at 300 °C, the main forms of N and S atoms in THFS molecules should be pyridine and thiophene. Due to their extremely low content in THFS (Table 2), their influence on the calculation of structural parameters of THFS can be negligible. Calculation of structural parameters indicates that the average molecule of THFS contains 15.8 total rings including 9.2 aromatic rings and 6.6 naphthenic rings. The σ of THFS is 0.56, indicating that THFS is primarily a complex aromatic species with a significant amount of substituents. This is consistent with its high aromatic carbon proportion in Table 5 and the low aromatic hydrogen proportion in Table 3. The σ_{al} of THFS is 0.32, indicating that the substituents are mainly alkyl substituents. The average molecule of THFS consists of 3.3 structural units with aromatic nuclei linked by methylene, naphthene, and so forth. Theoretically, low-molecular aromatic hydrocarbons and their derivatives can be produced by breaking these covalent bonds. The number of aromatic rings per average unit structure (or aromatic nucleus) is 2.8, which well agrees with the results of synchronous fluorescence spectroscopy. These results suggest that similar structures of

https://doi.org/10.1021/acsomega.3c01768
ACS Omega 2023, 8, 22820−22826

Table 6. Structural Parameters of THFS

parameter	definition	equation	value
f_a	aromaticity index	$f_a = C_{ar}/C_t$	0.57
H_{aru}	the maximum number of peripheral hydrogens in the hypothetical nucleus when all substituents (or bridges) have been replaced by hydrogen	$H_{aru} = H_{ar} + H_\alpha/2 + H_{ar-OH} + 2(O_{in} + N_t + S_t)$	32.4
σ	degree of substitution of the aromatic nucleus	$\sigma = [H_\alpha/2 + H_{ar-OH} + 2(O_{in} + N_t + S_t)]/H_{aru}$	0.56
σ_{al}	degree of aliphatic-chain substitution of the aromatic nucleus	$\sigma_{al} = (H_\alpha/2)/H_{aru}$	0.32
C_P	number of peripheral aromatic carbons	$C_P = H_{aru}$	32.4
C_I	number of internal aromatic carbons	$C_I = C_{ar} - C_P$	12.4
$C_{ar(us)}$	number of aromatic carbons per average unit structure	$C_{ar(us)} = 3/[H_{aru}/C_{ar} - 1/2]$	13.4
n	number of average units	$n = C_{ar}/C_{ar(us)}$	3.3
$C_{P(us)}$	number of peripheral aromatic carbons per average unit structure	$C_{P(us)} = C_{ar(us)} \times (H_{aru}/C_{ar})$	9.7
$R_{a(us)}$	aromatic rings per average unit structure	$R_{a(us)} = (C_{ar(us)} - C_{P(us)})/2 + 1$	2.8
R_a	total number of aromatic rings per molecule	$R_a = nR_{a(us)}$	9.2
R_t	total number of rings per molecule	$R_t = C_t - H_t/2 + 1 - C_{ar}/2$	15.8
R_n	total number of naphthene rings per molecule	$R_n = R_t - R_a$	6.6

THFS are presented in coal, and THFS is connected by the ether linkages destroyed by depolymerization.

4. CONCLUSIONS

To understand the structure of SDP and provide a theoretical basis for exploring the method of clean utilization of SDP, the structures of the subfraction of SDP were characterized in detail. The SDP obtained from the depolymerization of SL lignite consists of 10.4% of HS, 16.9% of TS, and 72.7% of THFS. Each subfraction of SDP is an aromatic derivative containing alkyl substituents and oxygen-containing functional groups. HS is a micromolecule containing abundant alkyl substituents and few oxygen-containing functional groups. TS and THFS are medium and large molecules containing plentiful oxygen-containing functional groups. The molecular weight of HS, TS, and THFS gradually increases, and the number of oxygen-containing functional groups and aromatic nuclei increases with their molecular weight. Depolymerization mainly destroys oxygen-containing functional groups but hardly affects the aromatic structure and alkyl structures; thus, SDP shows analogous structural features with lignite. Calculation of structural parameters by modified Brown–Ladner methods indicates that THFS is a complex macromolecule consisting of 3.3 average units with an average of 2.8 aromatic rings connected by bridge bonds. The average molecule of THFS contains about 15.8 total rings including 9.2 aromatic rings and 6.6 naphthenic rings. The σ and σ_{al} of THFS are 0.56 and 0.32, respectively, indicating plentiful substituents (alkyl substituents and oxygen-containing functional groups) in the aromatic nucleus of THFS. On average, each THFS molecule contains 6.1 alcohol hydroxyl groups, 3.9 phenol hydroxyl groups, 1.4 carboxyl groups, and 1.0 inactive oxygen-containing functional groups.

AUTHOR INFORMATION

Corresponding Authors

Jingchong Yan − *School of Chemistry & Chemical Engineering, Anhui Key Laboratory of Coal Clean Conversion & Utilization, Anhui University of Technology, Ma'anshan 243002 Anhui, P. R. China;* orcid.org/0000-0002-6628-2472; Email: jcyan@ahut.edu.cn

Hengfu Shui − *School of Chemistry & Chemical Engineering, Anhui Key Laboratory of Coal Clean Conversion & Utilization, Anhui University of Technology, Ma'anshan 243002 Anhui, P. R. China;* Email: shhf@ahut.edu.cn

Authors

Muxin Liu − *School of Materials and Chemical Engineering, Bengbu University, Bengbu 233030 Anhui, P. R. China; School of Chemistry & Chemical Engineering, Anhui Key Laboratory of Coal Clean Conversion & Utilization, Anhui University of Technology, Ma'anshan 243002 Anhui, P. R. China*

Zhiping Lei − *School of Chemistry & Chemical Engineering, Anhui Key Laboratory of Coal Clean Conversion & Utilization, Anhui University of Technology, Ma'anshan 243002 Anhui, P. R. China;* orcid.org/0000-0002-3219-0879

Xianzhong Cao − *School of Chemistry & Chemical Engineering, Anhui Key Laboratory of Coal Clean Conversion & Utilization, Anhui University of Technology, Ma'anshan 243002 Anhui, P. R. China*

Zhicai Wang − *School of Chemistry & Chemical Engineering, Anhui Key Laboratory of Coal Clean Conversion & Utilization, Anhui University of Technology, Ma'anshan 243002 Anhui, P. R. China;* orcid.org/0000-0002-3582-7935

Jiabao Hu − *School of Materials and Chemical Engineering, Bengbu University, Bengbu 233030 Anhui, P. R. China*

Mengqi Hong − *School of Materials and Chemical Engineering, Bengbu University, Bengbu 233030 Anhui, P. R. China*

Complete contact information is available at: https://pubs.acs.org/10.1021/acsomega.3c01768

Notes

The authors declare no competing financial interest.

ACKNOWLEDGMENTS

The authors gratefully acknowledge financial support from the National Natural Science Foundation of China (grants 21978003 and 22178001), Research Project for Outstanding Youth of the Department of Education of Anhui Province (2022AH030045), Excellent Young Talents Fund Program of Higher Education Institutions of Anhui Province (gxyqZD2022029), Key Project of Natural Science Research of Anhui Provincial Department of Education (KJ2021A1123, KJ2020ZD65, and 2022AH051910), Anhui Province Key Laboratory of Coal Clean Conversion and High Valued Utilization, Anhui University of Technology (grant CHV19-

https://doi.org/10.1021/acsomega.3c01768
ACS Omega 2023, 8, 22820−22826

03), and Key Project of Natural Science Research of Bengbu University (2022ZR02zd).

REFERENCES

(1) Lei, Z.; Liu, M.; Shui, H.; Wang, Z.; Wei, X. Study on the liquefaction of Shengli lignite with NaOH/methanol. *Fuel Process. Technol.* **2010**, *91*, 783−788.
(2) Okuyama, N.; Komatsu, N.; Shigehisa, T.; Kaneko, T.; Tsuruya, S. Hyper-coal process to produce the ash-free coal. *Fuel Process. Technol.* **2004**, *85*, 947−967.
(3) Koyano, K.; Takanohashi, T.; Saito, I. Catalytic hydrogenation of HyperCoal (ashless coal) and reusability of catalyst. *Energy Fuels* **2009**, *23*, 3652−3657.
(4) Yoshida, T.; Li, C.; Takanohashi, T.; Matsumura, A.; Sato, S.; Saito, I. Effect of extraction condition on "HyperCoal" production (2)—effect of polar solvents under hot filtration. *Fuel Process. Technol.* **2004**, *86*, 61−72.
(5) Shui, H.; Yao, J.; Wu, H.; Li, Z.; Yan, J.; Wang, Z.; Ren, S.; Lei, Z.; Chunbao Xu, C. Study on catalytic thermal dissolution of lignite and hydro-liquefaction of its soluble fraction for potential jet fuel. *Fuel* **2022**, *315*, 123237.
(6) Zou, D.; Yang, X.; Shui, H.; Wang, X.; Pan, C.; Wang, Z.; Lei, Z.; Ren, S.; Kang, S.; Li, Z.; Yan, J.; Xu, C. C. Liquefaction of thermal extracts from co-thermal dissolution of a sub-bituminous coal with lignin and reusability of Ni-Mo-S/Al_2O_3 catalyst. *J. Fuel Chem. Technol.* **2019**, *47*, 23−29.
(7) Wang, J.; Sakanishi, K.; Saito, I.; Takarada, T.; Morishita, K. High-yield hydrogen production by steam gasification of HyperCoal (ash-free coal extract) with potassium carbonate: comparison with raw coal. *Energy Fuels* **2005**, *19*, 2114−2120.
(8) Kawashima, H. Changes in sulfur functionality during solvent extraction of coal in HyperCoal production. *Fuel Process. Technol.* **2019**, *188*, 105−109.
(9) Takanohashi, T.; Shishido, T.; Saito, I. Effects of HyperCoal addition on coke strength and thermoplasticity of coal blends. *Energy Fuels* **2008**, *22*, 1779−1783.
(10) Zhao, J.; Zuo, H.; Wang, G.; Wang, J.; Xue, Q. Improving the coke property through adding HPC extracted from the mixture of low-rank coal and biomass. *Energy Fuels* **2020**, *34*, 1802−1810.
(11) Zhao, X.; Huang, S.; Cao, J.; Xi, S.; Wei, X.; Kamamoto, J.; Takarada, T. KOH activation of a HyperCoal to develop activated carbons for electric double-layer capacitors. *J. Anal. Appl. Pyrolysis* **2014**, *105*, 116−121.
(12) Ouchi, K.; Ozawa, H.; Makabe, M.; Ltoh, H. Dissolution of coal with NaOH-alcohol: Effect of alcohol species. *Fuel* **1981**, *60*, 474−476.
(13) Makabe, M.; Hirano, Y.; Ouchi, K. Extraction increase of coals treated with alcohol-sodium hydroxide at elevated temperatures. *Fuel* **1978**, *57*, 289−292.
(14) Bimer, J.; Salbut, P. D.; Berłożecki, S. Effect of chemical pretreatment on coal solubilization by methanol-NaOH. *Fuel* **1993**, *72*, 1063−1068.
(15) Liu, M.; Yang, J.; Yang, Y.; Liu, Z.; Shi, L.; He, W.; Liu, Q. The radical and bond cleavage behaviors of 14 coals during pyrolysis with 9,10-dihydrophenanthrene. *Fuel* **2016**, *182*, 480−486.
(16) Shui, H.; Yang, L.; Shui, T.; Pan, C.; Li, H.; Wang, Z.; Lei, Z.; Ren, S.; Kang, S. Hydro-liquefaction of thermal dissolution soluble fraction of Shenfu subbituminous coal and reusability of catalyst on the hydro-liquefaction. *Fuel* **2014**, *115*, 227−231.
(17) Ouchi, K.; Chicada, T.; Itoh, H. Pressure and temperature effect on the mean chemical structure of coal hydrogenolysis product. *Fuel* **1979**, *58*, 37−42.
(18) Yokoyama, S.; Bodily, D. M.; Wiser, W. H. Structural characterization of coal-hydrogenation products by proton and carbon-13 nuclear magnetic resonance. *Fuel* **1979**, *58*, 162−170.
(19) Zhang, J.; Niwamanya, N.; Gao, C.; Takyi Sekyere, D.; Barigye, A.; Tian, Y. Structure and millisecond pyrolysis behavior of heavy oil and its eight group-fractions on solid base catalyst. *Fuel* **2022**, *318*, 123483.
(20) Shao, R.; Shen, Z.; Li, D.; Sun, Z.; Pei, L.; Liu, X.; Li, W.; Dan, Y. Investigation on composition and structure of asphaltenes during low-temperature coal tar hydrotreatment under various reaction pressures. *J. Anal. Appl. Pyrolysis* **2018**, *136*, 44−52.
(21) Guo, X.; Xu, X.; Xue, X.; Li, X. Experimental investigation on the active sites during combustion of aromatic clusters in coals and chars. *J. Energy Inst.* **2022**, *104*, 133−141.
(22) Li, P.; Zong, Z.; Wei, X.; Wang, Y.; Fan, G. Structural features of liquefaction residue from Shenmu-Fugu subbituminous coal. *Fuel* **2019**, *242*, 819−827.
(23) Yan, Y.; Qi, Y.; Marshall, M.; Jackson, W. R.; Stanger, A.; Tran, Q. A.; Stanger, R.; Chaffee, A. L. Characterisation of coal density fractions separated from Victorian brown coal by reflux classification. *Fuel* **2021**, *292*, 120385.
(24) Wang, Z.; Wu, T.; Wu, Z.; Li, Z.; Yan, J.; Yan, H.; Pan, C.; Kang, S.; Lei, Z.; Ren, S.; Shui, H. A low carbon footprint method for converting low-rank coals to oxygen-containing chemicals. *Fuel* **2022**, *315*, 123277.
(25) Ma, Y.; Fan, X.; Mo, W.; Li, G.; Ma, F.; Wei, X. Catalytic hydrogenation and heteroatom removal for isopropanol soluble organic matter of Dongming lignite. *Fuel Process. Technol.* **2021**, *211*, 106589.
(26) Wang, J.; Tian, L.; Li, G.; Zhao, X.; Liang, Y.; Yu, J. Construction of vitrinite molecular structures based on ^{13}C NMR and FT-IR analysis: Fundamental insight into coal thermoplastic properties. *Fuel* **2021**, *300*, 120981.
(27) Katoh, T.; Yokoyama, S.; Sanada, Y. Analysis of a coal-derived liquid using highpressure liquid chromatography and synchronous fluorescence spectrometry. *Fuel* **1980**, *59*, 845−850.
(28) Wang, Z.; Wei, C.; Shui, H.; Ren, S.; Pan, C.; Wang, Z.; Li, H.; Lei, Z. Synchronous fluorimetric characterization of heavy intermediates of coal direct liquefaction. *Fuel* **2012**, *98*, 67−72.
(29) Sun, M.; Li, Y.; Sha, S.; Gao, J.; Wang, R.; Zhang, Y.; Hao, Q.; Chen, H.; Yao, Q.; Ma, X. The composition and structure of n-hexane insoluble-hot benzene soluble fraction and hot benzene insoluble fraction from low temperature coal tar. *Fuel* **2020**, *262*, 116511.
(30) Yan, J.; Bai, Z.; Bai, J.; Li, W. Chemical structure and reactivity alterations of brown coals during thermal treatment with aromatic solvents. *Fuel Process. Technol.* **2015**, *137*, 117−123.
(31) Guo, S.; Geng, W.; Yuan, S.; Yi, C.; Dong, Z.; Xu, J. Understanding the molecular structure of Datong coal by combining experimental and computational study. *J. Mol. Struct.* **2023**, *1279*, 135035.
(32) Shi, Q.; Li, C.; Wang, S.; Ji, R.; Xue, W.; Mi, Y.; Wang, S.; Cai, Y. Variation of molecular structures affecting tar yield: A comprehensive analysis on coal ranks and depositional environments. *Fuel* **2023**, *335*, 127050.
(33) Lu, J.; Wang, X.; Li, H.; Shi, S.; Yang, W.; Lu, Y.; Shao, S.; Ye, Q. Molecular insights into the methane adsorption capacity of coal under microwave irradiation based on solid-state 13C-NMR and XPS. *Fuel* **2023**, *339*, 127484.
(34) Zhu, Y.; Tian, F.; Liu, Y.; Cui, L.; Dan, Y.; Du, C.; Li, D. Comparison of the composition and structure for coal-derived and petroleum heavy subfraction by an improved separation method. *Fuel* **2021**, *292*, 120362.

https://doi.org/10.1021/acsomega.3c01768
ACS Omega 2023, 8, 22820−22826